Published in IET Electric Power Applications
Received on 14th September 2008
Revised on 8th April 2009
doi: 10.1049/iet-epa.2008.0227

ISSN 1751-8660

Sensored and sensorless speed control methods for brushless doubly fed reluctance motors

M. Jovanovic

School of Computing, Engineering and Information Sciences, Northumbria University, Ellison Building, Newcastle upon Tyne NE1 8ST, UK
E-mail: milutin.jovanovic@northumbria.ac.uk

Abstract: The study considers aspects of scalar V/f control, vector control and direct torque (and flux) control (DTC) of the brushless doubly fed reluctance machine (BDFRM) as a promising cost-effective alternative to the existing technological solutions for applications with restricted variable speed capability such as large pumps and wind turbine generators. Apart from providing a comprehensive literature review and analysis of these control methods, the development and results of experimental verification, of an angular velocity observer-based DTC scheme for sensorless speed control of the BDFRM which, unlike most of the other DTC-concept applications, can perform well down to zero supply frequency of the inverter-fed winding, have also been presented in the study.

1 Introduction

Although the inverter-fed brushless doubly fed reluctance machine (BDFRM) has not found any industrial use yet, it is no doubt an attractive low cost candidate for variable speed applications because of the high reliability of brushless structure, and lower harmonic injection into the supply mains. The economic benefits and improved power quality come from its slip power recovery property which allows the use of a smaller inverter (relative to the machine rating), and especially if the operating speed range required is limited (typical examples are large pumps and wind turbines [1–3]) when the inverter size and cost can be further reduced.

The BDFRM has two standard, sinusoidally distributed stator windings of generally different applied frequencies and pole numbers (Fig. 1). In order to provide rotor position-dependent magnetic coupling between the windings and torque production from the machine [4, 5], the reluctance rotor must have half the total number of stator poles. One implication of such an unusual operating principle [6] and unconventional design is the modest torque per volume so that a bigger, and therefore more expensive, BDFRM is needed to achieve the torque of an equivalent synchronous reluctance (SyncRel) or a cage induction machine (IM) [7]. Despite this deficiency, the total system cost can be substantially reduced in larger drives by significant savings in the power electronic hardware [8].

The BDFRM shares all the advantages of doubly fed machines (DFM) over singly excited cousins – the operational mode flexibility, the greater control freedom and the wider speed ranges, that is the possibility of sub-synchronous and super-synchronous operation in both motoring and generating regimes [7]. It can work as a conventional IM (which represents an important 'fail-safe' feature in case of the inverter failure) or as a fixed/adjustable speed synchronous turbo-machine [9] meaning that high-speed, field-weakened traction applications [10] and high-frequency generators [11] become feasible. From a control viewpoint, one important merit of the machine is that one can not only control its torque, but also the power factor (however, a larger inverter would be required in this case) [3, 12–14], efficiency [2] or any other performance parameter of interest in an inherently decoupled fashion [15].

When compared to machines of similar properties, the BDFRM is superior in many respects. The absence of brush

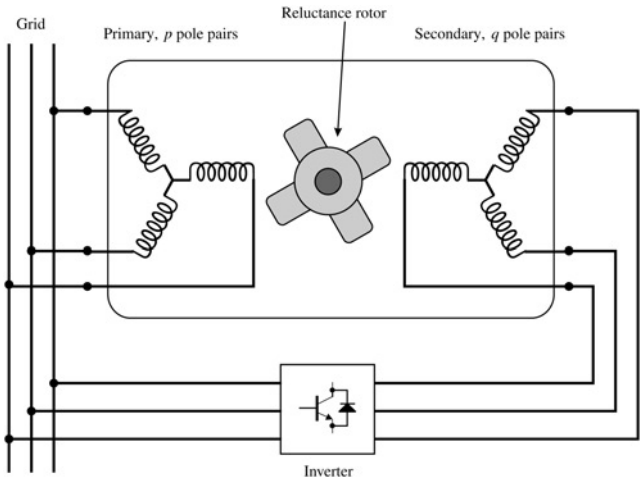

Figure 1 *Conceptual diagram of the inverter-fed BDFRM*

gear and slip rings is a clear advantage over a conventional doubly excited wound rotor induction machine (DEWRIM) in applications where increased reliability and lower maintenance requirements are crucial factors (for example, off-shore wind generators [16]). The BDFRM has higher efficiency [17], more robust construction and easier control than the closely related, brushless doubly fed induction machine (BDFIM) having the same stator as the BDFRM but replacing its cage-less reluctance rotor with a special cage one of 'nested' structure [18–21]. Recent studies have shown that with a rising rotor saliency-ratio, the BDFRM overall performance improves (as it does with the SyncRel) [7] to a level competitive with the IM [22]. The use of modern, commercially available SyncRel rotors is therefore a potentially viable (although not the most optimal) design solution which may have important cost reduction implications for the BDFRM manufacturing.

The primary intention of this paper is to provide a thorough review of the main control methodologies reported in the BDFRM literature. By integrating the existing control knowledge, this survey may serve as a useful up-to-date reference for future research on this particular machine. Algorithms for scalar control and direct torque (and flux) control (DTC) have already been proposed by the author and his co-workers and evaluated by computer simulations [2, 23] and experimentally [24, 25]. The same applies to the field-oriented control scheme, which has been simulated in [1] and later successfully practically implemented for both motoring and generating modes of the BDFRM [15]. However, these control approaches all rely on using encoder measurements for rotor position detection and/or speed identification. Eliminating a shaft position sensor would not only reduce the system cost but, more importantly, would further enhance the drive reliability in the target applications. The theoretical considerations presented in [26, 27] have concerned with sensorless field-oriented control and DTC, respectively. The simulation studies carried out in [14, 27] have been validated on a real machine for the first time in [3, 13, 14]. The test results from the latter conference papers have demonstrated how a rotor position/speed estimation technique and a conventional load model-based angular velocity observer [28] can be effectively used for accurate sensorless speed control down to synchronous speed (i.e. at zero secondary frequency) of the BDFRM. However, no journal publication has subsequently appeared to reinforce the originality, and significance of the practical verification, of the sensorless speed and DTC for the BDFRM operation at unity primary power factor achieved in [3, 13, 14]. This paper will attempt to fill this void by reproducing the major outcomes of this experimental work.

2 Dynamic modelling

The space-vector voltage and flux equations for the BDFRM in a stationary reference frame using standard notation and assuming motoring convention are [4, 6, 29]

$$\underline{u}_{p_s} = R_p \underline{i}_{p_s} + \frac{d\underline{\lambda}_{p_s}}{dt} = R_p \underline{i}_{p_s} + \left.\frac{d\underline{\lambda}_{p_s}}{dt}\right|_{\theta_p \text{const}} + j\omega_p \underline{\lambda}_{p_s} \quad (1)$$

$$\underline{u}_{s_s} = R_s \underline{i}_{s_s} + \frac{d\underline{\lambda}_{s_s}}{dt} = R_s \underline{i}_{s_s} + \left.\frac{d\underline{\lambda}_{s_s}}{dt}\right|_{\theta_s \text{const}} + j\omega_s \underline{\lambda}_{s_s} \quad (2)$$

$$\underline{\lambda}_{p_s} = L_p \underline{i}_{p_s} + L_{ps} \underline{i}^*_{s_s} e^{j\theta_r} \quad (3)$$

$$\underline{\lambda}_{s_s} = L_s \underline{i}_{s_s} + L_{ps} \underline{i}^*_{p_s} e^{j\theta_r} \quad (4)$$

The subscripts 'p' and 's' denote the primary (grid-connected) and secondary (inverter-fed) winding quantities, respectively, and '*' represents the complex conjugate. By omitting the exponential terms in (3) and (4), one obtains the rotating frame equivalents of (1)–(4) which, in a primary flux-oriented control form ($\lambda_{pq} = 0$), can be written as

$$\underline{u}_p = R_p \underline{i}_p + \frac{d\lambda_p}{dt} + j\omega_p \lambda_p \quad (5)$$

$$\underline{u}_s = R_s \underline{i}_s + \frac{d\underline{\lambda}_s}{dt} + j\omega_s \underline{\lambda}_s \quad (6)$$

$$\lambda_p = L_p \underline{i}_p + L_{ps} \underline{i}^*_s \quad (7)$$

$$\underline{\lambda}_s = L_s \underline{i}_s + L_{ps} \underline{i}^*_p = \sigma L_s \underline{i}_s + \underbrace{\frac{L_{ps}}{L_p} \lambda_p}_{\lambda_{ps}} \quad (8)$$

where $\sigma = 1 - L^2_{ps}/(L_p L_s) = 1 - k^2_{ps}$ is the leakage factor (defined as with the IM), $k_{ps} = L_{ps}/\sqrt{L_p L_s}$ is the coupling coefficient between the windings (as in the power transformer case), $L_{p,s,ps}$ are the respective three-phase inductances [4, 7], and λ_{ps} is the primary flux linking the secondary winding, that is the mutual flux (Fig. 2).

Applying the fundamental BDFRM theory [4, 6, 29], one can establish the following condition for the machine

doi: 10.1049/iet-epa.2008.0227

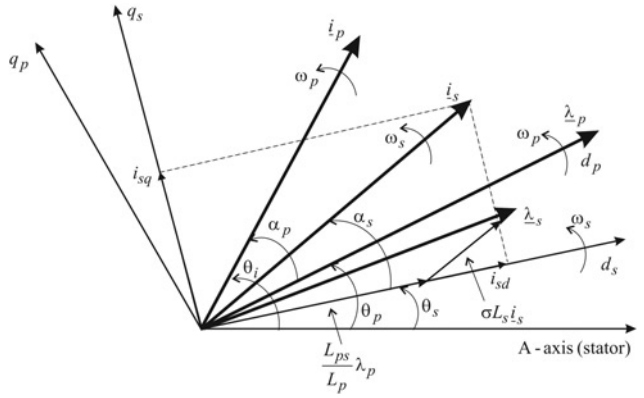

Figure 2 *Reference frames and characteristic phasors*

torque production

$$\omega_r = p_r\omega_{rm} = \omega_p + \omega_s \Longleftrightarrow \theta_r = p_r\theta_{rm} = \theta_p + \theta_s \quad (9)$$

where $\omega_{rm} = d\theta_{rm}/dt$ is the rotor mechanical angular velocity (rad/s), p_r is the number of rotor poles (equal to the sum of the windings pole pairs, that is $p + q$ according to Fig. 1), $\omega_{p,s} = d\theta_{p,s}/dt$ are the applied angular frequencies (rad/s) to the windings and $\theta_{r,p,s}$ are the angular positions of the rotating reference frames (it has been assumed that the two windings are accommodated in the same slots so that there is no space displacement between the respective phase axes) as illustrated in Fig. 2 (the rotor frame is omitted for convenience). Notice that $\omega_s > 0$ for 'super-synchronous' ($\omega_{rm} > \omega_{syn}$) and $\omega_s < 0$ for 'sub-synchronous' ($\omega_{rm} < \omega_{syn}$) machine operation. The BDFRM synchronous speed, $\omega_{syn} = \omega_p/p_r$, occurs with the DC secondary winding, that is when $\omega_s = 0$. The 'negative' secondary frequency at sub-synchronous speeds simply means the opposite phase sequence of the secondary to the primary winding.

It should be emphasised that the primary equations, (5) and (7), and secondary equations, (6) and (8), are in two different reference frames – d_pq_p and d_sq_s rotating at ω_p and $\omega_s = \omega_r - \omega_p$, respectively. If one arbitrary chose the primary d_pq_p frame to be aligned with the λ_p vector (since this is of fixed frequency and approximately constant magnitude because of the primary winding grid connection), then the secondary d_sq_s frame would lie along the λ_{ps} vector as shown in Fig. 2. Note from the same figure that the λ_s and λ_{ps} vectors are mutually stationary (they both rotate at ω_s), and for the machine to produce average torque there must be a phase shift between them as will be elaborated later in the DTC section.

3 Scalar control

In pump-type drives, simple, parameter-independent scalar control may be a suitable solution as steady-state, and not dynamic, performance of a machine is of main concern. Furthermore, the speed ranges, and therefore the frequency variations in these systems are usually limited which mitigates the open-loop stability problems commonly associated with this method in case of sudden step changes of the desired frequency.

The V/f = const control strategy (Fig. 3), first proposed in [2], is by no means optimal and has been primarily developed by analogy with the conventional IM to illustrate the 'proof of concept'. In keeping with this assumption, the supply voltage boost, normally present in general purpose IM drives to compensate for resistive voltage drops and improve torque production at lower speeds, has not been implemented in the controller either.

The BDFRM can be started as a slip ring IM (with the shorted secondary winding). Once when vicinity of synchronous speed is reached, the inverter is connected and the control enabled. Note that an auxiliary contactor, normally used for this purpose, is not shown in Fig. 3. Such a starting procedure is required to prevent the current overloading of the fractionally rated inverter during start-up. An alternative approach could be to start the machine with the shorted primary windings by means of the controllable inverter and then self-synchronise it to the grid for doubly fed operation, by applying a starting method similar to that used for commercial DEWRIM drives [30].

The results obtained by executing the algorithm in Fig. 3 have been presented in [2, 24] and will not be repeated here. They have demonstrated the satisfactory controller performance over the speed range of interest to the BDFRM target applications. With open-loop control at f_p = 50 Hz line frequency, the shaft speed of the BDFRM prototype (see Appendix for specifications) can be varied stably within a narrow range (600–900 rpm) around the synchronous speed (750 rpm). The corresponding secondary frequency, f_s, band is (−10, 10) Hz according to (9). The rate of change of f_s reference signal obviously affects the transient performance and stability of the system. The above figures have been obtained by testing the machine response

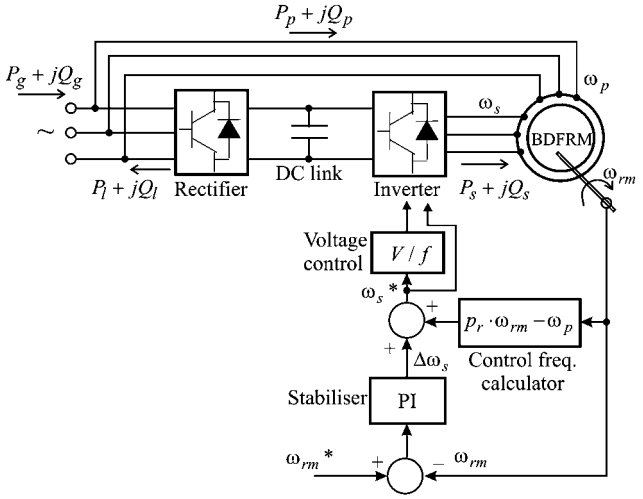

Figure 3 *Structure of a BDFRM drive with scalar control*

to sudden (step) changes of f_s, and by manually tuning the PI controller gains, that is applying a simple 'trial and error' method. Smoother and slower f_s variations (like a ramp transition) should increase the stability margin. The closed-loop control has expectedly provided a wider controllable speed range of 400–1100 rpm with the respective f_s limits of $-/+23.33$ Hz, which may be quite sufficient for pump-type applications and geared wind turbines where the machine speed ratios of approximately 2:1 (i.e. 500–1000 rpm, and $f_s = f_p/3$) are typically encountered.

4 Vector control

As for any other machine, this high-performance model-based control method allows much faster transient response compared to the scalar control, but an accurate knowledge of the BDFRM parameters, which can be obtained by off-line testing or estimated on-line, is necessary. For this reason, vector control algorithms are more complicated and hence computationally more intensive (among other things, because of the reference frame conversion requirement) than scalar control counterparts so that DSP implementation is imperative (unlike the latter which can be implemented on a micro-controller) to achieve high control rates. Furthermore, for most AC machines, special decoupling schemes are required to eliminate cross-coupling effects between the $d-q$ rotating frame control axes. In this sense, one important advantage of the BDFRM (and DEWRIM) is the inherently decoupled control of torque (T_e) and primary winding reactive power (Q_p). The secondary real power (P_s), T_e and Q_p in a primary flux-oriented control frame can be expressed as [4, 15]

$$P_s = \frac{\omega_s}{\omega_p + \omega_s} P_{out} = \frac{\omega_s}{\omega_p} P_p \tag{10}$$

$$T_e = \frac{P_{out}}{\omega_{rm}} = \frac{3}{2} p_r \frac{L_{ps}}{L_p} \lambda_p i_{sq} \tag{11}$$

$$Q_p = \frac{3}{2} \frac{\omega_p \lambda_p}{L_p} (\lambda_p - L_{ps} i_{sd}) \tag{12}$$

As can be seen from (11) and (12), T_e is controlled by the secondary q-axis current, i_{sq}, and Q_p by the secondary d-axis current, i_{sd}, and there is no coupling between the two expressions (since λ_p is virtually constant). Note also that the machine slip power recovery property is hidden in (10). For example, if the secondary is supplied at the line frequency (i.e. $\omega_s = \omega_p$), the inverter has to handle at most half the output power (plus losses). However, if $\omega_s = 0.25\omega_p$, then the secondary winding contribution to the machine power production is only 20%. Therefore in applications where the BDFRM would have to operate in a narrow range around the synchronous speed when ω_s values are small, a partially rated inverter could be used as mentioned earlier.

The structure of a typical BDFRM drive with vector control based on (11) and (12) is shown in Fig. 4 [15].

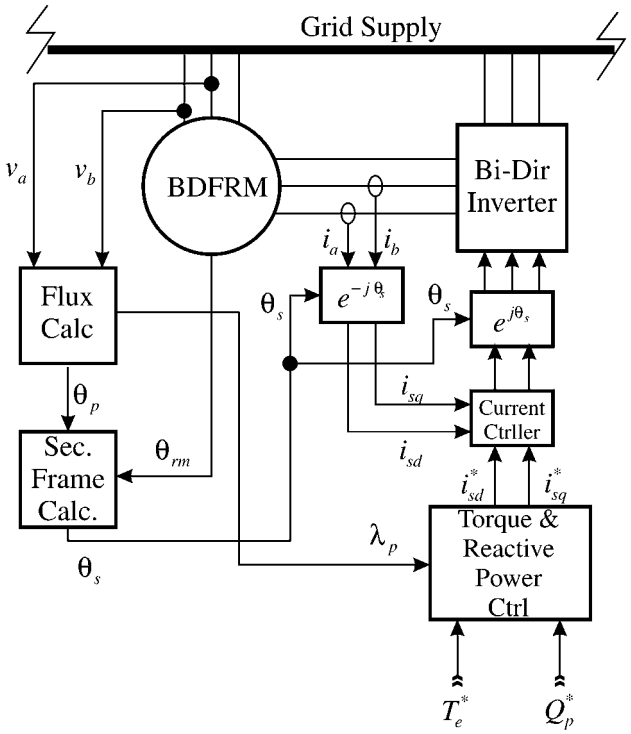

Figure 4 *Simplified block diagram of the field-oriented torque controller for the BDFRM*

Considering that only the secondary winding quantities are controllable, one should first identify the secondary frame position (θ_s) using (9). The rotor position, θ_{rm}, is usually detected by a shaft sensor while the primary flux angle (Fig. 2), θ_p, follows from

$$\underline{\lambda}_{p_s} = \lambda_p e^{j\theta_p} = \int (\underline{u}_{p_s} - R_p \underline{i}_{p_s}) dt \simeq \int \underline{u}_{p_s} dt \tag{13}$$

where $\underline{u}_{p_s}$ and $\underline{i}_{p_s}$ can be easily determined from the measured phase quantities. It should be mentioned that the resistive voltage drop in (13) can be neglected with larger machines having inherently lower resistances and dominant back-emf values. Once θ_s is known one can implement current control of the secondary $d_s q_s$ components (and thus T_e and Q_p) in a traditional manner (Fig. 4) to optimise a desired performance parameter of the machine such as [2, 24]: (i) the maximum torque per secondary (inverter) ampere (i.e. $i_{sd} = 0$) [7, 12]; (ii) the maximum primary power factor (i.e. $i_{sd} = \lambda_p / L_{ps}$ for $Q_p = 0$) [12, 15]; (iii) the unity line power factor (i.e. $Q_g = 0$ and $Q_l = Q_p$ in Fig. 3) [12]; (iv) the minimum copper losses for improved efficiency [12] and so forth.

Finally, in keeping with the power factor control abilities of the BDFRM, notice that while it is perfectly true that power factor correction on the mains side is possible by varying the secondary excitation it comes at the price of considerable copper loss and an increased current rating requirement on the supply inverter [12]. Therefore the potential reductions in inverter size (and hence, cost) may not be fully realisable in view of VAr flows. This efficiency against power factor

doi: 10.1049/iet-epa.2008.0227

performance trade-off that exists in the BDFRM (and the DEWRIM) opens up a wide scope of opportunities for further research on both the machines.

5 Direct torque control

5.1 Generalities

Since its original development for cage IMs [31, 32], the DTC concept, by virtue of its versatility, fewer machine parameter dependence and fast dynamic response (control sampling frequencies of at least 10 KHz are common), has been successfully used for torque and stator flux control of almost all brushless machines for high-performance drives. These apparent advantages, coupled with the absence of current control loops, make it clearly superior to vector (or field oriented) control with high and variable switching rates (and consequent torque ripples, higher core losses and therefore compromised efficiency) representing its obvious limitations. However, until very recently, the DTC application to DFMs in general has been relatively little reported in the refereed literature. An alternative rotor frame-based DTC technique for the BDFIM required a shaft position sensor for torque control and it was very complex even for DSP implementation [33]. DTC schemes presented in [34–36] for a conventional doubly fed induction generator (DFIG), on the other hand, have only been studied by computer simulations. In the last couple of years, predictive DTC strategies of constant switching frequency have been proposed and experimentally verified for the DEWRIM but used an encoder for control purposes [37–39]. Except for the author's practical work on the BDFRM control [13, 14], the only other test validation of sensorless DTC for DFMs has appeared in [40]. While a viable, parameter-independent DTC algorithm for unity power factor control of the DFIG in wind power applications has been developed, the sustained synchronous speed operation of the machine has not been clearly demonstrated.

It is well-known that back-emf-based control approaches, including DTC, have low-frequency stability problems because of flux estimation inaccuracies caused by resistance variations at lower supply voltages (under these operating conditions DTC is clearly inferior to vector control). It is mainly for this reason that this control method has been extremely popular for high-speed drive systems where the resistance effects are less pronounced making the DTC virtually parameter independent and as such preferable to vector control in these applications. Fortunately, the common difficulties of traditional DTC at low secondary frequencies can be overcome in the BDFRM as both its windings are accessible externally, which allows more freedom in parameter identification and control as will be shown in the following.

5.2 Main principles

One of the key issues of the DTC application to the BDFRM is how to control the secondary flux to achieve desired torque dynamics. An answer to this question can be found in (8) and a DTC form of (11)

$$\underline{\lambda}_s = \lambda_{sd} + j\lambda_{sq} = \sigma L_s i_{sd} + \lambda_{ps} + j\sigma L_s i_{sq} \tag{14}$$

$$T_e = \frac{3p_r}{2\sigma L_s}|\underline{\lambda}_{ps} \times \underline{\lambda}_s| = \frac{3p_r}{2\sigma L_s}\underbrace{\frac{L_{ps}}{L_p}\lambda_p}_{\lambda_{ps}}\lambda_s \sin\delta \tag{15}$$

It is evident from (14) and (11) that λ_{sq} is a torque producing secondary flux component since it is directly proportional to i_{sq}. Therefore in order to increase (decrease) instantaneous torque for a given λ_s, one needs to apply appropriate voltage vectors to the secondary winding to allow the secondary flux angle in the d_sq_s frame (Fig. 2), that is δ in (15), to increase (decrease). This effectively means that the respective stationary frame angle, $\delta + \theta_s$, would also change accordingly as θ_s variations are negligible (and especially at low ω_s values) over a short control interval dictated by the inherently high DTC sampling rates. There is obviously no need to know the secondary frame position at all, and the DTC can be implemented in a stator frame as usual for this method.

The outputs of the flux and torque comparators in the DTC algorithm developed for the BDFRM (Fig. 5) can be defined as

$$\Delta\lambda_s = \begin{cases} 1, & \lambda_s^* - \lambda_s \geq \Delta\lambda \\ 0, & \lambda_s^* - \lambda_s \leq -\Delta\lambda \end{cases} \tag{16}$$

$$\Delta T_e = \begin{cases} 1, & T_e^* - T_e \geq \Delta T \\ 0, & T_e^* - T_e \leq 0,\ \omega_s \geq 0 \\ 0, & T_e^* - T_e \geq 0,\ \omega_s \leq 0 \\ -1, & T_e^* - T_e \leq -\Delta T \end{cases} \tag{17}$$

where ΔT and $\Delta\lambda$ indicate a half width of the corresponding hysteresis bands. The secondary voltage vectors generated by the inverter to achieve a desired control action with the

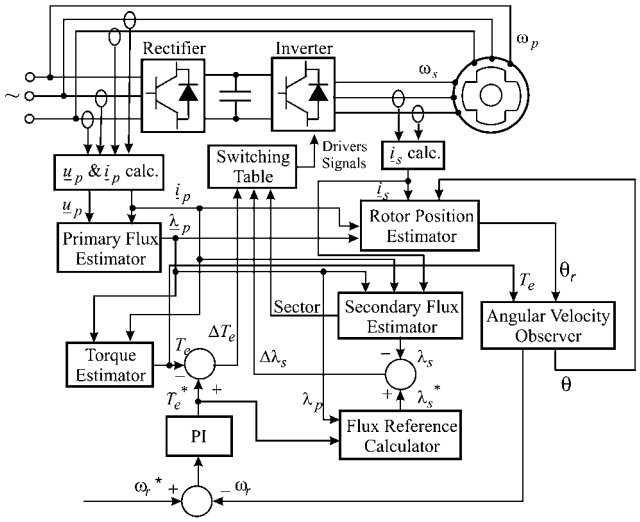

Figure 5 *Sensorless BDFRM drive with DTC*

minimum number of switchings are given in Table 1. The binary codes, indicating the switching status of individual inverter legs (with '1' representing the top device of a leg ON and bottom OFF, and '0' vice versa) and angular positions of these vectors in a stationary frame are presented in Fig. 6.

The controller main task is to ensure that the secondary flux and machine torque are kept within the user-specified hysteresis bands under all operating conditions of the machine. In the flux case, according to (16), the λ_s values should be in the range $[\lambda_s^* - \Delta\lambda, \lambda_s^* + \Delta\lambda]$ with $\Delta\lambda_s = 1$ voltage vectors increasing, and $\Delta\lambda_s = 0$ vectors decreasing the λ_s magnitudes (Table 1). Similarly in (17), $\Delta T_e = 1$ means the increase, and $\Delta T_e = -1$ the decrease of actual (not absolute) torque which is assumed positive if acting counterclockwise as in Fig. 2. However, the influence of zero voltage vectors ($\underline{U}_0 = 000$ and $\underline{U}_7 = 111$) on torque behaviour is opposite above and below the synchronous speed of the BDFRM: at super-synchronous speeds they reduce torque, and at sub-synchronous speeds they increase torque (again in actual, not absolute, sense) as follows from Table 2. As a result, in the super-synchronous speed region, the torque is controlled in the bottom half-band $[T_e^* - \Delta T, T_e^*]$, and in the sub-synchronous mode, in the top half-band $[T_e^*, T_e^* + \Delta T]$. Therefore unlike (16) the use of zero vectors imposes speed dependence of (17) and complicates torque control, especially for synchronous speed operation of the machine when the rate of change of secondary current (and hence torque) and control quality would be poor due to the lack of back-emf caused by $\omega_s = 0$ (refer to [23, 27] for further details). For this reason, the switching strategy adopted in this paper is based on the active voltage vectors only and knowledge of the machine speed is not required in the proposed DTC scheme (Fig. 5).

It is interesting to note that despite the fundamentally different operating principles there is a close similarity of Table 1 for the BDFRM to the switching look-up table used for DTC of cage IMs [31, 32, 41]. In super-synchronous mode, as shown in Fig. 2, the d_pq_p and d_sq_s frames rotate in the same 'anti-clockwise' (positive) direction at ω_p and $\omega_s > 0$, respectively, as the induction motor counterparts do.

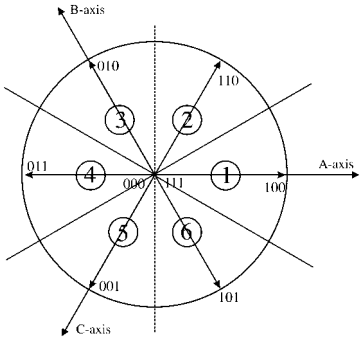

Figure 6 *Secondary voltage vectors ($\underline{U}_0 = 000$, $\underline{U}_1 = 100$, $\underline{U}_2 = 110$, $\underline{U}_3 = 010$, $\underline{U}_4 = 011$, $\underline{U}_5 = 001$, $\underline{U}_6 = 101$ and $\underline{U}_7 = 111$) and associated $\pi/3$ sectors*

Table 2 Effects of voltage vectors on BDFRM torque

ω_s	ΔT_e	Torque changes	
		$\omega_{rm} > 0$	$\omega_{rm} < 0$
>0	1	↗	↗
	0	↘	↗
	−1	↘	↘
<0	1	↗	↗
	0	↗	↘
	−1	↘	↘

However, at sub-synchronous speeds, the BDFRM speed and torque are again of the same sign (both positive or negative), so that mechanical power is being delivered to the load, but the d_sq_s frame and associated phasors now rotate 'clockwise' (due to the opposite phase sequence of the secondary winding to the primary in this speed region), and $\omega_s < 0$ in (9). In this mode, which is analogous to regenerative braking in IMs (the principal difference being that the BDFRM operation can be sustained), the secondary supply voltage will simply reverse its polarity to allow power regeneration through the secondary winding for the machine operating as a motor as

Table 1 Optimum switching look-up table

Comparator		Sector					
$\Delta\lambda_s$	ΔT_e	1	2	3	4	5	6
1	1	$\underline{U}_2$	$\underline{U}_3$	$\underline{U}_4$	$\underline{U}_5$	$\underline{U}_6$	$\underline{U}_1$
	0	$\underline{U}_7$	$\underline{U}_0$	$\underline{U}_7$	$\underline{U}_0$	$\underline{U}_7$	$\underline{U}_0$
	−1	$\underline{U}_6$	$\underline{U}_1$	$\underline{U}_2$	$\underline{U}_3$	$\underline{U}_4$	$\underline{U}_5$
0	1	$\underline{U}_3$	$\underline{U}_4$	$\underline{U}_5$	$\underline{U}_6$	$\underline{U}_1$	$\underline{U}_2$
	0	$\underline{U}_0$	$\underline{U}_7$	$\underline{U}_0$	$\underline{U}_7$	$\underline{U}_0$	$\underline{U}_7$
	−1	$\underline{U}_5$	$\underline{U}_6$	$\underline{U}_1$	$\underline{U}_2$	$\underline{U}_3$	$\underline{U}_4$

doi: 10.1049/iet-epa.2008.0227

follows from (10) for $\omega_s < 0$. The relative positions of the λ_s and mutual flux, λ_{ps}, phasors remain unchanged though to allow 'motoring' torque to be produced by the machine according to (15).

5.3 Secondary flux estimation

As discussed earlier, the use of (2) for estimating the secondary flux magnitude and stationary frame angle is not convenient in the low-frequency region. Considering that both the primary and secondary quantities are measurable in the BDFRM, the following alternative expression can be derived using (1), (3) and (4)

$$\underline{\lambda}_{s_s} = L_s \underline{i}_{s_s} + \underline{i}^*_{p_s} \frac{\underline{\lambda}_{p_s} - L_p \underline{i}_{p_s}}{\underline{i}^*_{s_s}} \tag{18}$$

where $\underline{\lambda}_{p_s}$ is given by (13) but taking into account the resistive voltage drop to minimise the primary flux estimation errors as the BDFRM prototype considered is small and has larger resistances [25]. The magnitudes and angular positions of $\underline{i}_{s_s}$ and $\underline{i}_{p_s}$ can be calculated from measurements [23, 25, 27]. Applying (18) one would obviously avoid the voltage integration and related problems but at the expense of having to know the winding self-inductances $L_{p,s}$.

5.4 Rotor position and speed estimation

For the scope of this paper, another significant benefit of greater control freedom, afforded by the accessibility of both BDFRM windings, is the possibility of sensorless speed control [27]. The rotor angle, θ_r, can be retrieved from (3) as follows

$$\left.\begin{aligned} \theta_{r_1} &= \tan^{-1} \frac{\mathrm{Im}[(\underline{\lambda}_p - L_p \underline{i}_p)\underline{i}_s]}{\mathrm{Re}[(\underline{\lambda}_p - L_p \underline{i}_p)\underline{i}_s]} \\ \theta_{r_1} &= \theta_{r_2} + \pi \end{aligned}\right\} \tag{19}$$

The raw position estimates are then input to a Luenberger-type PI observer [28] to predict the rotor angular velocity $\omega_r = \mathrm{d}\theta/\mathrm{d}t$ used for the speed control as shown in Fig. 5. An excellent dynamic response and low-pass filtering abilities of this observer, anticipated by simulations in [27], have been experimentally verified by the results presented in the following.

5.5 Torque estimation

There are many equivalent torque expressions for the BDFRM, the one best suited to control purposes being

$$T_e = \frac{3}{2} p_r |\underline{\lambda}_{p_s} \times \underline{i}_{p_s}| = \frac{3}{2} p_r (\lambda_{pd} i_{pq} - \lambda_{pq} i_{pd}) \tag{20}$$

where the subscripts 'pd' and 'pq' indicate the respective stator frame components (Fig. 2) of $\underline{\lambda}_{p_s}$ and $\underline{i}_{p_s}$. High estimation accuracy can be achieved in practice as (20) is nearly machine parameter independent (except for indirect R_p effects through λ_p estimates) and is based on the primary quantities having 'clean' waveforms at fixed line frequency. Switching ripples, which are present on the secondary waveforms, are virtually non-existent on the primary side because of the inherently weak magnetic coupling between the windings.

6 Experimental results

The sensorless control algorithm in Fig. 5 was executed in dSPACE® on a small 6/2-pole BDFRM prototype [23, 25] (refer to Appendix for details) at 10 kHz sampling rate. The observed speed estimates (and the speed controller output i.e. desired torque values) were updated at 2 kHz which was fast enough for the drive system inertia. The lower speed control rate has also added benefits in improving the quality of rotor position and speed estimation as discussed below. The preliminary tests were conducted for the unloaded machine as the main objective was to assess the controller viability.

The plots in Fig. 7 represent the rotor angles (θ_r) obtained from (19), and their absolute variations from encoder measurements. Note that a shaft position sensor was used simply for monitoring purposes and not for control. For this reason, it is not shown in Fig. 5. The raw estimates, θ_r, are notably noisy, the error spikes being occasionally larger than 30°. Despite these ripples, which have been found to be mainly because of the practical effects such as measurement noise and quantisation as well as sensitivity to parameter knowledge inaccuracies, the average estimation error is still reasonably low (≃7°).

The effectiveness of the observer as a low-pass filter is evident from Fig. 8, and a significant improvement in accuracy is achieved by processing θ_r. The average error is reduced to approximately 1.5° with the maximum values

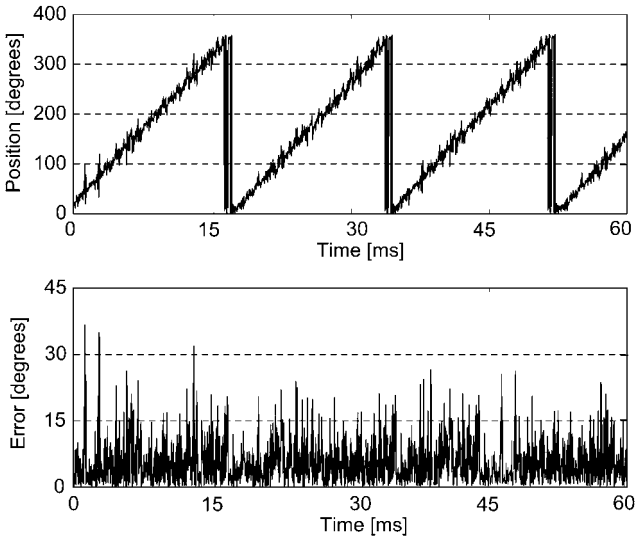

Figure 7 *Estimated position and estimator absolute errors at 850 rpm (f_s =6.7 Hz)*

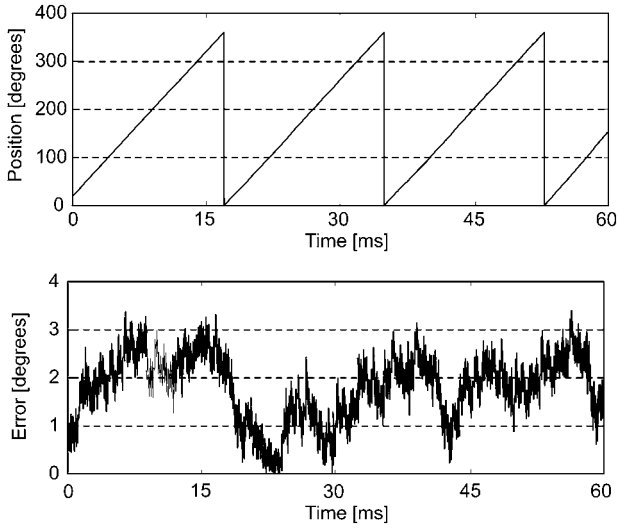

Figure 8 *Observed position and observer errors corresponding to Fig. 7*

being about 3.4° or less. The main reason for such accuracy are the high quality estimates being fed into the observer by the position estimator which, similarly to the latter, works in a closed-loop fashion as illustrated in Fig. 5. The observer last prediction, θ, has served as a reference while selecting the best out of the ten raw estimates available per 500 μs speed control interval (as there are two possible solutions for θ_r according to (19) calculated each 100 μs) that is the one having the least absolute deviation from θ. Therefore the estimator block itself carries out the first filtering of noisy θ_r before inputting the best estimate to the observer for further processing. The filtered θ_r values are plotted out in Fig. 7.

In order to demonstrate the validity and high accuracy of the sensorless algorithm in a limited speed range around synchronous speed (750 rpm) at low secondary frequencies (f_s), the machine was operated in super- and sub-synchronous modes at $f_s = 6.7$ Hz. The respective speed waveform in Fig. 9 clearly illustrates the good controller performance with very little overshoot under transient conditions.

Fig. 10 shows similar results to Fig. 9 but for changing desired speed values between 950, 750 and 550 rpm. In this case, the speed limits correspond to $f_s \simeq 13.3$ Hz in either mode. It can be seen that the machine can be effectively controlled over the considered speed range, including synchronous speed (750 rpm) when $f_s = 0$. The reliable low-frequency operation of the BDFRM is an important merit of the proposed sensorless scheme, and certainly represents a significant advantage over traditional DTC and many other back-emf-based control methods having difficulties (or simply not working) in this frequency region even in sensor speed mode. It should be emphasised that the gains of both the speed PI regulator and the observer must be lowered and appropriately tuned as

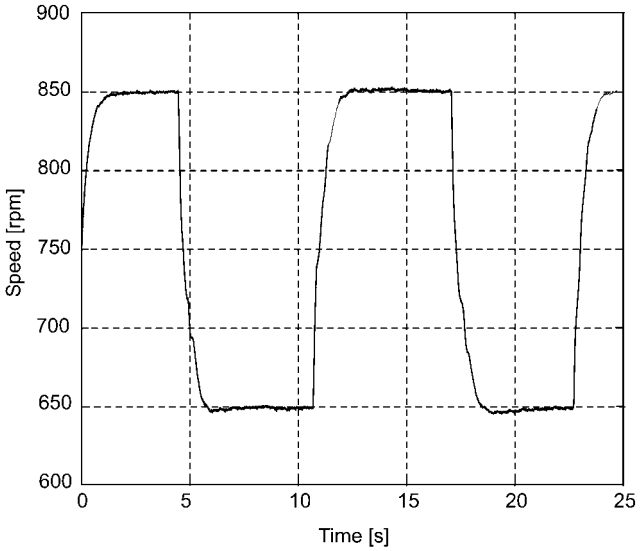

Figure 9 *BDFRM response to a varying speed reference between 850 and 650 rpm*

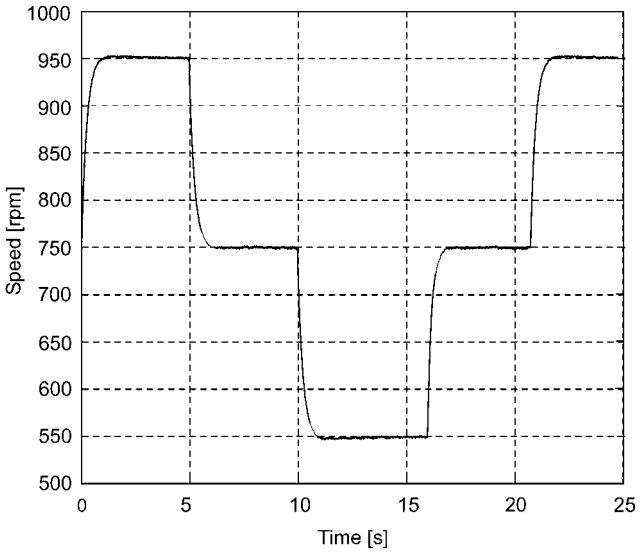

Figure 10 *Sensorless control performance down to synchronous speed*

instability and divergency of the control algorithm may otherwise occur due to noisy input estimates. This trade-off results in low bandwidth control and relatively modest dynamic response of the machine which, fortunately, is quite acceptable for the target applications where steady-state performance is of more interest.

7 Conclusions

The fundamental principles and implementation aspects of different control techniques for the BDFRM have been surveyed in this paper. This kind of unified study can be extremely helpful for control development and research on this interesting and unusual slip-power recovery machine.

doi: 10.1049/iet-epa.2008.0227

A similar control-related framework for the BDFRM or any other DFM has not been published in the refereed literature to date.

The paper has looked at the classical speed control methods which have been applied to other AC motors such as: scalar control, field-oriented control and finally, DTC. Except for the vector control, the remaining algorithms considered have been developed by the author and his colleagues, and most of them, including the vector control one, use rotor position measurements for control. In addition to making a comprehensive review of the existing BDFRM control literature, details of successful real-time implementation of a sensorless speed control scheme with DTC have also been presented in the paper as one of the most important achievements hitherto published on the subject. The experimental results generated for the unloaded BDFRM prototype have demonstrated good controller performance down to zero frequency of the inverter-fed (secondary) winding this being difficult to achieve with many other machines controlled either with or without a shaft position sensor.

The main advantages of the sensorless control algorithm and the associated estimation techniques are:

- Applicability over the entire speed range of the machine down to synchronous speed. This property makes the proposed DTC scheme competitive with field-oriented control in the low-frequency range.

- The rotor position is estimated on-line at the control rate allowing the controller to effectively replace the encoder readings.

- The injection of any special signals or special inverter switching strategies are not required unlike with many other sensorless methods.

- The high instantaneous accuracy of both the position predictions and angular velocity estimates at any speed can be attributed to the use of a standard load model-based observer and the secondary flux/torque estimation approach where measurements of grid-connected winding quantities at fixed line frequency, and not the inverter outputs or DC link voltage, have been used for control calculations.

- The proposed estimation methods are versatile and can serve as a basis for sensorless vector control where an accurate rotor position knowledge is needed.

Further tests are currently in progress to evaluate the controller performance for different loading conditions of the machine.

Possible directions for future control research on the BDFRM could include the development of: (i) improved, more realistic dynamic models and associated compensated torque control strategies to account for iron loss effects the machine is susceptible to by the nature of its unusual operating principle; (ii) appropriate power factor control techniques to minimise the related efficiency trade-offs in terms of increased copper losses; (iii) alternative robust secondary flux observer configurations to avoid (or at least reduce) the machine parameter dependence of the proposed DTC scheme making it advantageous to field-oriented control in the target applications; (iv) algorithms for on-line parameter estimation of the machine and so on.

8 References

[1] XU L., TANG Y.: 'A novel wind-power generating system using field orientation controlled doubly-excited brushless reluctance machine'. Proc. IEEE IAS Annual Meeting, October 1992, vol. 1, pp. 408–413

[2] JOVANOVIĆ M.G., BETZ R.E., YU J.: 'The use of doubly fed reluctance machines for large pumps and wind turbines', *IEEE Trans. Ind. Appl.*, 2002, **38**, pp. 1508–1516

[3] DORRELL D.G., JOVANOVIĆ M.: 'On the possibilities of using a brushless doubly-fed reluctance generator in a 2 MW wind turbine'. IEEE Industry Applications Society Annual Meeting (IAS), 5–9 October 2008, pp. 1–8

[4] BETZ R.E., JOVANOVIĆ M.G.: 'Introduction to the space vector modelling of the brushless doubly-fed reluctance machine', *Electric Power Compon. Syst.*, 2003, **31**, pp. 729–755

[5] BETZ R.E., JOVANOVIĆ M.G.: 'Theoretical analysis of control properties for the brushless doubly fed reluctance machine', *IEEE Trans. Energy Convers.*, 2002, **17**, pp. 332–339

[6] LIAO Y., XU L., ZHEN L.: 'Design of a doubly-fed reluctance motor for adjustable speed drives', *IEEE Trans. Ind. Appl.*, 1996, **32**, pp. 1195–1203

[7] BETZ R.E., JOVANOVIĆ M.G.: 'The brushless doubly fed reluctance machine and the synchronous reluctance machine – a comparison', *IEEE Trans. Ind. Appl.*, 2000, **36**, pp. 1103–1110

[8] LIAO Y.: 'Design of a brushless doubly-fed induction motor for adjustable speed drive applications'. Proc. IEEE IAS Annual Meeting, October 1996, pp. 850–855

[9] OJO O., WU Z.: 'Synchronous operation of a dual-winding reluctance generator', *IEEE Trans. Energy Convers.*, 1997, **12**, pp. 357–362

[10] SAIFKHANI F., WALLACE A.K.: 'A linear brushless doubly-fed machine drive for traction applications'. Proc. European Power Electronics Conf., September 1993, pp. 344–348

[11] WALLACE A.K., SPEE R., ALEXANDER G.C.: 'Adjustable speed drive and variable speed generation systems with reduced power converter requirements'. Proc. Int. Symp. Industrial Electronics (ISIE), 1993, pp. 503–508

[12] JOVANOVIĆ M.G., BETZ R.E.: 'Power factor control using brushless doubly fed reluctance machines'. Proc. IEEE-IAS Annual Meeting, October 2000, vol. 1, pp. 523–530

[13] JOVANOVIĆ M.G., AHMED M.M.R.: 'Sensorless speed control strategy for brushless doubly-fed reluctance machines'. Electric Machines and Drives Conf. (IEMDC), 3–5 May 2007, vol. 2, pp. 1514–1519

[14] JOVANOVIĆ M.G., DORRELL D.G.: 'Sensorless control of brushless doubly-fed reluctance machines using an angular velocity observer', *Power Electron. Drive Syst. (PEDS)*, 2007, pp. 717–724

[15] XU L., ZHEN L., KIM E.: 'Field-orientation control of a doubly excited brushless reluctance machine', *IEEE Trans. Ind. Appl.*, 1998, **34**, pp. 148–155

[16] BAUER P., DE HAAN S., MEYL C.R., PIERIK J.T.G.: 'Evaluation of electrical systems for off-shore windfarms'. Proc. IEEE IAS Annual Meeting, October 2000, vol. 3, pp. 1416–1423

[17] WANG F., ZHANG F., XU L.: 'Parameter and performance comparison of doubly-fed brushless machine with cage and reluctance rotors', *IEEE Trans. Ind. Appl.*, 2002, **38**, pp. 1237–1243

[18] WILLIAMSON S., FERREIRA A., WALLACE A.: 'Generalised theory of the brushless doubly-fed machine. Part 1: analysis', *IEE Proc.-Electr. Power Appl.*, 1997, **144**, pp. 111–122

[19] ROBERTS P.C., MCMAHON R.A., TAVNER P.J., MACIEJOWSKI J.M., FLACK T.J.: 'Equivalent circuit for the brushless doubly fed machine (BDFM) including parameter estimation and experimental verification', *IEE Proc.-Electr. Power Appl.*, 2005, **152**, pp. 933–942

[20] MCMAHON R.A., ROBERTS P.C., WANG X., TAVNER P.J.: 'Performance of BDFM as generator and motor', *IEE Proc.-Electr. Power Appl.*, 2006, **153**, pp. 289–299

[21] POZA J., OYARBIDE E., ROYE D., RODRIGUEZ M.: 'Unified reference frame dq model of the brushless doubly fed machine', *IEE Proc.-Electr. Power Appl.*, 2006, **153**, pp. 726–734

[22] SCHULZ E.M., BETZ R.E.: 'Optimal torque per amp for brushless doubly fed reluctance machines'. Proc. IEEE IAS Annual Meeting, October 2005, vol. 3, pp. 1749–1753

[23] JOVANOVIĆ M.G., YU J., LEVI E.: 'Direct torque control of brushless doubly fed reluctance machines', *Electric, Power Compon. Syst.*, 2004, **32**, pp. 941–958

[24] JOVANOVIĆ M.: 'Control of brushless doubly-fed reluctance motors'. Proc. Int. Symp. on Industrial Electronics, 2005, vol. 4, pp. 1667–1672

[25] JOVANOVIĆ M.G., YU J., LEVI E.: 'Encoderless direct torque controller for limited speed range applications of brushless doubly fed reluctance motors', *IEEE Trans. Ind. Appl.*, 2006, **42**, pp. 712–722

[26] LIAO Y., SUN C.: 'A novel position sensorless control scheme for doubly fed reluctance motor drives', *IEEE Trans. Ind. Appl.*, 1994, **30**, pp. 1210–1218

[27] JOVANOVIĆ M.G., YU J., LEVI E.: 'A doubly-fed reluctance motor drive with sensorless direct torque control'. Proc. IEEE Int. Electric Machines and Drives Conf. (IEMDC), June 2003, vol. 3, pp. 1518–1524

[28] LORENZ R., PATTEN K.: 'High-resolution velocity estimation for all-digital, ac servo drives', *IEEE Trans. Ind. Appl.*, 1991, **IA-27**, pp. 701–705

[29] LIANG F., XU L., LIPO T.: 'D-q analysis of a variable speed doubly AC excited reluctance motor', *Electric Mach. Power Syst.*, 1991, **19**, pp. 125–138

[30] MOREL L., GODFROID H., MIRZAIAN A., KAUFFMANN J.M.: 'Double-fed induction machine: converter optimisation and field oriented control without position sensor', *IEE Proc. – Electr. Power Appl.*, 1998, **145**, pp. 360–368

[31] TAKAHASHI I., NOGUCHI T.: 'A new quick-response and high-efficiency control strategy of an induction machine', *IEEE Trans. Ind. Appl.*, 1986, **IA-22**, pp. 820–827

[32] TAKAHASHI I., OHMORI Y.: 'High performance direct torque control of an induction motor', *IEEE Trans. Ind. Appl.*, 1989, **25**, pp. 257–264

[33] BRASSFIELD W.R., SPEE R., HABETLER T.G.: 'Direct torque control for brushless doubly-fed machines', *IEEE Trans. Ind. Appl.*, 1996, **32**, (5), pp. 1098–1104

[34] ARNALTE S., BURGOS J.C., RODRIGUEZ-AMENEDO J.L.: 'Direct torque control of a doubly-fed induction generator for variable speed wind turbines', *Electric Power Compon. Syst.*, 2002, **30**, pp. 199–216

[35] XU L., CARTWRIGHT P.: 'Direct active and reactive power control of DFIG for wind energy generation', *IEEE Trans. Energy Convers.*, 2006, **21**, pp. 750–758

[36] ZHI D., XU L.: 'Direct power control of DFIG with constant switching frequency and improved transient performance', *IEEE Trans. Energy Convers.*, 2007, **22**, pp. 110–118

[37] ABAD G., RODRIGUEZ M.A., POZA J.: 'Two-level VSC-based predictive direct torque control of the doubly fed

doi: 10.1049/iet-epa.2008.0227

induction machine with reduced power ripple at low constant switching frequency', *IEEE Trans. Energy Convers.*, 2008, **23**, pp. 570–580

[38] ABAD G., RODRIGUEZ M.A., POZA J.: 'Three-level NPC converter-based predictive direct power control of the doubly fed induction machine at low constant switching frequency', *IEEE Trans. Ind. Electron.*, 2008, **55**, pp. 4417–4429

[39] ABAD G., RODRIGUEZ M.A., POZA J.: 'Two-level VSC based predictive direct torque control of the doubly fed induction machine with reduced torque and flux ripples at low constant switching frequency', *IEEE Trans. Power Electron.*, 2008, **23**, pp. 1050–1061

[40] DATTA R., RANGANATHAN V.T.: 'Direct power control of grid-connected wound rotor induction machine without rotor position sensors', *IEEE Trans. Power Electron.*, 2001, **16**, pp. 390–399

[41] VAS P.: 'Sensorless vector and direct torque control' (Oxford University Press, 1998)

9 Appendix

9.1 BDFRM test system specifications

The laboratory test rig for the 'proof-of-concept' BDFRM driving an 'off-the-shelf' DC load machine is presented in Fig. 11. The six-pole primary and two-pole secondary windings are both rated at 2.5 A, 415 V, 50 Hz. The four-pole axially-laminated reluctance rotor [23] and the stator have been custom designed and built. The rotor design is not optimal as the main focus of the project being undertaken has been on the control aspects. A standard

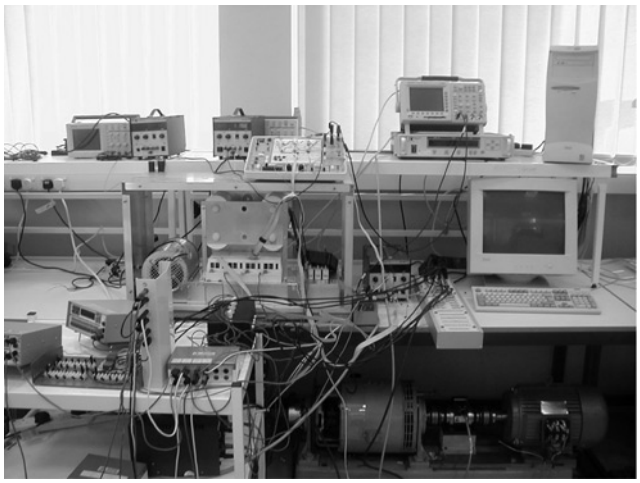

Figure 11 *Experimental test system for the BDFRM*

IGBT inverter supplying the secondary winding is controlled by a high-performance DS1103 PPC controller board from dSPACE®. An incremental encoder with 5000 ppr (increased to 20 000 ppr by the four-fold pulse counting), mounted on the DC side of the drive, has been used for shaft position sensing and speed detection.

The BDFRM parameters of importance for the control have been identified by applying off-line testing methods for conventional slip ring induction machines [17]. The actual resistances (measured by a simple DC test) and three-phase inductances of the windings are: $R_p = 10.7\ \Omega$, $R_s = 12.68\ \Omega$, $L_p = 0.407$ H, $L_s = 1.256$ H and $L_{ps} = 0.57$ H. The values are somewhat higher than usual mainly because of the small gage copper wire employed and consequent larger number of turns of the windings (especially the secondary).